ELSEVIER

International Journal of Mass Spectrometry 185/186/187 (1999) 359–380

International Journal of Mass Spectrometry

Absolute alkali metal ion binding affinities of several azoles determined by threshold collision-induced dissociation

M.T. Rodgers[a,*], P.B. Armentrout[b]

[a]*Department of Chemistry, Wayne State University, Detroit, MI 48202, USA*
[b]*Department of Chemistry, University of Utah, Salt Lake City, UT 84112, USA*

Received 5 June 1998; accepted 3 August 1998

Abstract

Collision-induced dissociation of M^+(azole) with xenon is studied using guided ion beam mass spectrometry. M^+ include the following alkali metal ions: Li^+, Na^+ and K^+. The azoles studied include imidazole, 1,2,4-triazole, 1,2,3-triazole, and tetrazole. In all cases, the primary product formed corresponds to endothermic loss of the intact azole. The cross-section thresholds are interpreted to yield 0 and 298 K bond energies for M^+(azole) after accounting for the effects of multiple ion-molecule collisions, internal energy of the reactant ions, and dissociation lifetimes. The possibility that the triazoles and tetrazole tautomerize during the formation of the complexes and during their dissociation is explicitly considered. Ab initio calculations at the 6-31G** level are used to help assign the observed thresholds to specific dissociation processes. We find that the kinetically favored (thermodynamically less stable) complex is formed in all cases, indicating that tautomerization barriers in the presence of the metal ions are appreciable. (Int J Mass Spectrom 185/186/187 (1999) 359–380) © 1999 Elsevier Science B.V.

Keywords: Alkali metal ions; Azoles; Binding affinities; Collision-induced dissociation; Guided ion beams; Tautomerization

1. Introduction

In recent work, we have developed methods to allow the application of quantitative threshold collision-induced dissociation methods to obtain accurate thermodynamic information on increasingly large systems [1–3]. One of the driving forces behind these developments is our interest in applying such techniques to systems having biological relevance. In the present paper, we examine the interactions of the family of five-membered heterocycles containing nitrogen, the azoles, with alkali ions. These systems were chosen as models of noncovalent interactions with nucleic acids and possibly of selective cation transport through biological membranes [4,5]. The azoles are building blocks for many antibiotics, anticancer agents, and drugs used in the treatment of AIDS [6–8]. Tetrazoles are used as promoters for synthesis of a variety of biopolymers [9,10]. The large nitrogen content also makes the azoles important as high energy density compounds useful in explosives and fuels [11,12] and as clean sources of nitrogen in thin film deposition [13–15].

In the present study, we use guided ion beam mass spectrometry to collisionally excite complexes of Li^+,

* Corresponding author.

In honor of Michael T. Bowers on the occasion of his 60th birthday and in thanks for his many contributions to gas-phase ion chemistry.

PII S1387-3806(98)14134-9

Na^+, and K^+ bound to four different azoles: imidazole (*c*-$C_3H_4N_2$), 1,2,4-triazole (*c*-$C_2H_3N_3$), 1,2,3-triazole (*c*-$C_2H_3N_3$) and tetrazole (*c*-CH_2N_4). The kinetic energy dependent cross sections for the collision-induced dissociation (CID) processes are analyzed using methods developed previously [3]. The analysis explicitly includes the effects of the internal and translational energy distributions of the reactants, multiple collisions, and the lifetime for dissociation. We derive metal cation-azole bond dissociation energies for all the complexes and compare these results to relative values available for Li^+ obtained in equilibrium studies [16] and to ab initio calculations performed here and in the literature [17–19].

One of the interesting aspects of the azoles is their propensity to tautomerize. The various possible structures are shown in Fig. 1. For instance, tetrazole is supplied as a solid of the 1*H*-tautomer, but experiments [20,21] indicate that the most stable gas-phase structure is the 2*H*-tautomer. Analogously, 1,2,3-triazole is supplied as a solid of the 1*H*-tautomer, while the 2*H*-1,2,3-triazole has been measured to dominate the gas-phase species by a factor of 1000 [22]. In contrast, 1*H*-1,2,4-triazole is the most stable structure in both the gas-phase [23,24] and solid state [25,26], but can tautomerize to the 4*H*-1,2,4-tautomer. As the vaporization of the solid azoles could yield both tautomers in the gas phase and complexation of the vaporized neutral azoles with alkali ions may provide sufficient energy to overcome any barriers to tautomerization, the ground state structures of the alkali ion complexes might correspond to binding of the alkali ions to any of the tautomeric forms. There is also the interesting question of whether the azole ligand might tautomerize upon collision-induced dissociation of the alkali ion complexes. These possibilities are considered explicitly below.

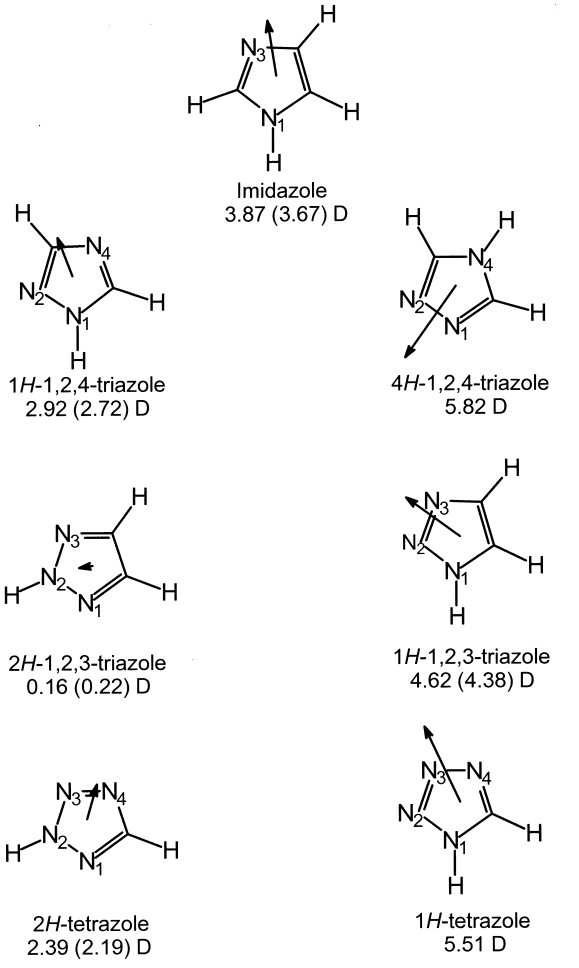

Fig. 1. Structures of the azole molecules, including both tautomers of the triazoles and tetrazoles. The most stable gas phase tautomer is on the left, while metal ions are calculated to bind more tightly to the tautomers on the right (see text). Properly scaled dipole moments in Debye are shown as arrows. Values listed are taken from theory (Ref. [57]) and experiment (in parentheses, Refs. [20, 22–24, and 58]).

2. Experimental

2.1. General procedures

Cross sections for CID of M^+(azole), where M^+ = Li^+, Na^+ and K^+, and azole = imidazole, 1,2,3-triazole, 1,2-4-triazole and tetrazole, are measured using a guided ion beam mass spectrometer that has been described in detail previously [27,28]. The metal ligand complexes are generated as described below. The ions are extracted from the source, accelerated, and focused into a magnetic sector momentum analyzer for mass analysis. Mass-selected ions are decelerated to a desired kinetic energy and focused into an octopole ion guide, which traps the ions in the radial

direction [29]. The octopole passes through a static gas cell containing xenon, used as the collision gas, for reasons described elsewhere [30–32]. Low gas pressures in the cell (typically 0.04 to 0.20 mTorr) are used to ensure that multiple ion-molecule collisions are improbable. Product and unreacted beam ions drift to the end of the octopole where they are focused into a quadrupole mass filter for mass analysis and subsequently detected with a secondary electron scintillation detector and standard pulse counting techniques.

Ion intensities are converted to absolute cross sections as described previously [27]. Absolute uncertainties in cross section magnitudes are estimated to be ±20%, which are largely the result of error in the pressure measurement and the length of the interaction region. Relative uncertainties are approximately ±5%. Because the radio frequency used for the octopole does not trap light masses with high efficiency, the cross sections for Li^+ products were more scattered and showed more variations in magnitude than is typical for this apparatus. Therefore, absolute magnitudes of the cross sections for production of Li^+ are probably ±50%.

Ion kinetic energies in the laboratory frame, E_{lab}, are converted to energies in the center of mass frame, E_{CM}, using the formula $E_{CM} = E_{lab}\, m/(m + M)$, where M and m are the masses of the ionic and neutral reactants, respectively. All energies reported below are in the CM frame unless otherwise noted. The absolute zero and distribution of the ion kinetic energies are determined using the octopole ion guide as a retarding potential analyzer as previously described [27]. The distribution of ion kinetic energies is nearly Gaussian with a full width at half maximum (FWHM) typically between 0.2 and 0.3 eV (lab) for these experiments. The uncertainty in the absolute energy scale is ±0.05 eV (lab).

Even when the pressure of the reactant neutral is low, we have previously demonstrated that the effects of multiple collisions can significantly influence the shape of CID cross sections [33]. Because the presence and magnitude of these pressure effects is difficult to predict, we have performed pressure dependent studies of all cross sections examined here. In the present systems, we observe small cross sections at low energies that have an obvious dependence upon pressure. We attribute this to multiple energizing collisions that lead to an enhanced probability of dissociation below threshold as a result of the longer residence time of these slower moving ions. Data free from pressure effects is obtained by extrapolating to zero reactant pressure, as described previously [33]. Thus, results reported below are the result of single bimolecular encounters.

2.2. Ion source

The M^+(azole) complexes are formed in a 1 m long flow tube [28,34] operating at a pressure of 0.5–0.7 Torr with a helium flow rate of 4000–7000 sccm. Metal ions are generated in a continuous dc discharge by argon ion sputtering of a cathode, made from tantalum or iron, with a cavity containing the alkali metal. Typical operating conditions of the discharge are 2–3 kV and 20–30 mA in a flow of roughly 10% argon in helium. The M^+(azole) complexes are formed by associative reactions of the alkali metal ion with the neutral azole, which is introduced into the flow 50 cm downstream from the dc discharge. The azoles are vaporized by gently heating and flowing helium over the sample. We might expect that the most stable gas phase tautomer of the neutral azole is formed in the vaporization process. This would imply that 1*H*-1,2,3-triazole and 1*H*-tetrazole undergo tautomerization during vaporization, whereas the 1*H*-1,2,4-triazole does not. However, we have no direct means of establishing which tautomer is formed during vaporization. Therefore in our data analysis, we explicitly consider all possible tautomers for the metallated complexes and neutral azole products. The flow conditions used in this ion source provide in excess of 10^4 collisions between an ion and the buffer gas, which should thermalize the ions both vibrationally and rotationally. In our analysis of the data, we assume that the ions produced in this source are in their ground electronic states and that the internal energy of the M^+(azole) complexes is well described by a Maxwell-Boltzmann distribution of ro-vibrational states at 300 K. Previous work from

this laboratory has shown that these assumptions are generally valid [30,33–38].

2.3. Thermochemical analysis

The threshold regions of the reaction cross sections are modeled using Eq. (1),

$$\sigma(E) = \sigma_0 \sum_i g_i(E + E_i - E_0)^n/E \quad (1)$$

where σ_0 is an energy independent scaling factor, E is the relative translational energy of the reactants, E_0 is the threshold for reaction of the ground electronic and ro-vibrational state, and n is an adjustable parameter. The summation is over the ro-vibrational states of the reactant ions, i, where E_i is the excitation energy of each state and g_i, is the population of those states ($\sum g_i = 1$). The populations of excited ro-vibrational levels are not negligible even at 300 K as a result of the many low-frequency modes present in these ions. The relative reactivities of all ro-vibrational states, as reflected by σ_0 and n, are assumed to be equivalent.

Ab initio calculations were performed with Hyperchem to obtain model structures, energetics, and vibrational frequencies for the neutral, protonated and metallated azoles. In all calculations, the starting structures are annealed and then energy minimized at low levels of theory (semi-empirical, STO-3G, 3-21G and 6-31G*) to obtain good starting structures for the final geometry optimization calculations performed at the HF 6-31G** level [39]. A vibrational analysis of the final geometry-optimized structures is then performed to determine the vibrational frequencies and rotational constants of the molecules. We scale the vibrational frequencies obtained in our analyses by a factor of 0.9 as suggested by recent work [40,41]. The scaled vibrational frequencies thus obtained are listed in Table 1, while Table 2 lists the rotational constants. The Beyer-Swinehart algorithm [42] is used to evaluate the density of the ro-vibrational states and the relative populations g_i are calculated by an appropriate Maxwell-Boltzmann distribution at the 300 K temperature appropriate for the reactants.

The average vibrational energy at 298 K of the alkali metal ion bound azoles is also given in Table 1. We have estimated the sensitivity of our analysis to the deviations from the true frequencies by scaling the originally calculated 6-31G** frequencies to encompass the range of average valence coordinate scale factors needed to bring calculated frequencies into agreement with experimentally determined frequencies found by Seeger et al. [40] and Pople et al. [43]. The originally calculated vibrational frequencies were scaled by 0.7 and 1.1. The corresponding change in the average vibrational energy is taken to be an estimate of one standard deviation of the uncertainty in vibrational energy and is included in the uncertainties listed with the E_0 values.

We also consider the possibility that collisionally activated complex ions do not dissociate on the time scale of our experiment (about 10^{-4} s) by including statistical theories for unimolecular dissociation into Eq. (1) as described in detail elsewhere [3,35]. This requires sets of ro-vibrational frequencies appropriate for the energized molecules and the transition states (TSs) leading to dissociation. The former are given in Tables 1 and 2 although we assume that the TSs are loose and product-like because the interaction between the alkali metal ion and the ligand is largely electrostatic. In this case, the TS vibrations used are the frequencies corresponding to the products, which are also found Table 1. The transitional frequencies, those that become rotations of the completely dissociated products, are treated as rotors, a treatment that corresponds to a phase space limit (PSL) and is described in detail elsewhere [3]. For the M^+(azole) complexes, the two transitional mode rotors have rotational constants equal to those of the neutral azole product with axes perpendicular to the reaction coordinate. These are listed in Table 2. The external rotations of the energized molecule and TS are also included in the modeling of the CID data. The external rotational constants of the TS are determined by assuming that the TS state occurs at the centrifugal barrier for interaction of M^+ with the neutral azole, calculated variationally as outlined elsewhere [3]. The 2-D external rotations are treated adiabatically but with centrifugal effects included consistent with the discussion of Waage and Rabinovitch [44]. In the present work, we used the statistical assumption with

Table 1
Vibrational frequencies and average vibrational energies at 298 K[a]

Species	E_{vib}, eV[b]	Frequencies, cm^{-1}
Imidazole	0.07 (0.02)	491, 623, 659, 757, 872, 885, 902, 918, 1039, 1068, 1109, 1128, 1267, 1353, 1427, 1498, 1569, 3079, 3082, 3111, 3538
Li^+(imidazole)	0.10 (0.02)	126, 172, **473**, 599, 635, 669, 779, 901, 907, 915, 935, 1050, 1088, 1107, 1162, 1275, 1331, 1444, 1526, 1572, 3093, 3095, 3127, 3501
Na^+(imidazole)	0.12 (0.02)	83, 105, **232**, 591, 632, 666, 777, 893, 904, 910, 924, 1051, 1090, 1103, 1153, 1275, 1337, 1440, 1520, 1570, 3088, 3091, 3125, 3508
K^+(imidazole)	0.12 (0.02)	64, 75, **156**, 581, 629, 665, 776, 887, 901, 907, 922, 1050, 1090, 1100, 1148, 1275, 1341, 1437, 1517, 1569, 3083, 3088, 3124, 3513
1*H*-1,2,4-triazole	0.06 (0.01)	538, 661, 680, 915, 940, 946, 966, 1058, 1114, 1151, 1265, 1312, 1411, 1475, 1585, 3093, 3100, 3542
Li^+(1*H*-1,2,4-triazole)	0.10 (0.02)	134, 180, **457**, 625, 674, 698, 929, 941, 952, 987, 1065, 1123, 1164, 1273, 1289, 1437, 1509, 1590, 3103, 3107, 3496
Na^+(1*H*-1,2,4-triazole)	0.11 (0.02)	90, 111, **221**, 620, 677, 689, 928, 936, 954, 974, 1068, 1127, 1158, 1273, 1292, 1432, 1501, 1588, 3099, 3104, 3505
K^+(1*H*-1,2,4-triazole)	0.12 (0.02)	69, 81, **144**, 613, 678, 683, 926, 932, 954, 971, 1068, 1129, 1154, 1273, 1298, 1428, 1495, 1587, 3098, 3102, 3512
4*H*-1,2,4-triazole	0.06 (0.02)	501, 641, 681, 865, 889, 925, 954, 1038, 1072, 1078, 1222, 1318, 1414, 1545, 1552, 3103, 3106, 3538
Li^+(4*H*-1,2,4-triazole)	0.10 (0.02)	148, 198, **460**, 611, 663, 673, 922, 939, 943, 961, 1022, 1095, 1103, 1228, 1338, 1412, 1555, 1575, 3113, 3119, 3488
Na^+(4*H*-1,2,4-triazole)	0.11 (0.02)	102, 122, **239**, 603, 653, 675, 914, 932, 941, 957, 1027, 1093, 1099, 1226, 1332, 1413, 1553, 1568, 3114, 3116, 3499
K^+(4*H*-1,2,4-triazole)	0.12 (0.02)	88, 108, **169**, 595, 651, 678, 906, 926, 939, 956, 1029, 1093, 1097, 1226, 1328, 1415, 1551, 1564, 3111, 3116, 3504
1*H*-1,2,3-triazole	0.06 (0.02)	574, 648, 720, 799, 897, 938, 966, 1043, 1089, 1126, 1150, 1345, 1386, 1445, 1558, 3108, 3127, 3537
Li^+(1*H*-1,2,3-triazole)	0.10 (0.02)	102, 137, **443**, 629, 691, 731, 832, 933, 951, 979, 1072, 1098, 1150, 1204, 1324, 1394, 1453, 1554, 3116, 3133, 3483
Na^+(1*H*-1,2,3-triazole)	0.11 (0.02)	82, 96, **227**, 628, 681, 728, 826, 927, 947, 977, 1070, 1099, 1142, 1190, 1322, 1394, 1452, 1554, 3116, 3133, 3495
K^+(1*H*-1,2,3-triazole)	0.12 (0.02)	83, 86, **158**, 624, 669, 726, 821, 923, 945, 975, 1068, 1100, 1139, 1182, 1325, 1394, 1452, 1555, 3118, 3134, 3508
2*H*-1,2,3-triazole	0.06 (0.02)	550, 670, 713, 856, 916, 945, 968, 1038, 1137, 1155, 1264, 1295, 1426, 1440, 1567, 3096, 3112, 3544
Li^+(2*H*-1,2,3-triazole)	0.10 (0.02)	113, 177, **430**, 533, 657, 701, 863, 941, 941, 995, 1050, 1132, 1161, 1264, 1288, 1418, 1470, 1563, 3096, 3123, 3512
Na^+(2*H*-1,2,3-triazole)	0.11 (0.02)	72, 108, **206**, 531, 661, 704, 862, 936, 942, 984, 1049, 1133, 1157, 1272, 1285, 1420, 1463, 1566, 3095, 3122, 3521
K^+(2*H*-1,2,3-triazole)	0.12 (0.02)	57, 80, **128**, 532, 663, 706, 860, 930, 942, 978, 1046, 1133, 1155, 1273, 1285, 1421, 1458, 1567, 3094, 3122, 3529
1*H*-tetrazole	0.06 (0.01)	569, 676, 733, 912, 982, 1002, 1061, 1080, 1134, 1284, 1395, 1466, 1549, 3121, 3538
Li^+(1*H*-tetrazole)	0.10 (0.02)	138, 144, **412**, 651, 711, 736, 950, 995, 1012, 1090, 1104, 1133, 1293, 1422, 1480, 1558, 3125, 3477
Na^+(1*H*-tetrazole)	0.11 (0.02)	93, 102, **216**, 647, 701, 736, 944, 994, 1008, 1088, 1103, 1135, 1290, 1415, 1476, 1555, 3126, 3489
K^+(1*H*-tetrazole)	0.11 (0.02)	85, 87, **146**, 642, 695, 736, 939, 993, 1006, 1085, 1099, 1135, 1288, 1410, 1475, 1553, 3127, 3498
2*H*-tetrazole	0.06 (0.01)	613, 706, 737, 921, 998, 1029, 1107, 1154, 1192, 1298, 1326, 1432, 1566, 3130, 3531
Li^+(2*H*-tetrazole)	0.10 (0.02)	133, 141, **436**, 691, 716, 772, 936, 1005, 1048, 1132, 1153, 1260, 1268, 1338, 1439, 1571, 3132, 3470
Na^+(2*H*-tetrazole)	0.11 (0.02)	53, 95, **215**, 687, 712, 759, 933, 1003, 1042, 1129, 1155, 1239, 1275, 1338, 1432, 1537, 3135, 3480
K^+(2*H*-tetrazole)	0.11 (0.02)	56, 81, **144**, 678, 709, 751, 931, 1001, 1040, 1128, 1156, 1224, 1280, 1339, 1429, 1565, 3134, 3493

[a] Vibrational frequencies are obtained from a vibrational analysis of the geometry optimized structures for these species obtained from ab initio calculations performed at the 6-31G** level after scaling by 0.9. The reaction coordinate is indicated in boldface.
[b] Uncertainties listed in parentheses are determined as described in the text.

Table 2
Rotational constants of M^+(azole) in cm^{-1}

	Energized molecule		Transition state	
Reactant	1-D[a]	2-D[b]	1-D[c]	2-D[d]
Li^+(imidazole)	0.33	0.12	0.16, 0.32, 0.33	0.039
Na^+(imidazole)	0.33	0.059	0.16, 0.32, 0.33	0.0085
K^+(imidazole)	0.33	0.037	0.16, 0.32, 0.33	0.0055
Li^+(1*H*-1,2,4-triazole)	0.34	0.13	0.17, 0.34, 0.35	0.044
Na^+(1*H*-1,2,4-triazole)	0.34	0.059	0.17, 0.34, 0.35	0.0094
K^+(1*H*-1,2,4-triazole)	0.35	0.037	0.17, 0.34, 0.35	0.0058
Li^+(4*H*-1,2,4-triazole)	0.34	0.14	0.17, 0.34, 0.34	0.039
Na^+(4*H*-1,2,4-triazole)	0.34	0.069	0.17, 0.34, 0.34	0.0081
K^+(4*H*-1,2,4-triazole)	0.34	0.043	0.17, 0.34, 0.34	0.0049
Li^+(1*H*-1,2,3-triazole)	0.34	0.14	0.17, 0.34, 0.34	0.032
Na^+(1*H*-1,2,3-triazole)	0.34	0.067	0.17, 0.34, 0.34	0.0071
K^+(1*H*-1,2,3-triazole)	0.34	0.042	0.17, 0.34, 0.34	0.0042
Li^+(2*H*-1,2,3-triazole)	0.35	0.13	0.17, 0.34, 0.35	0.035
Na^+(2*H*-1,2,3-triazole)	0.35	0.060	0.17, 0.34, 0.35	0.0079
K^+(2*H*-1,2,3-triazole)	0.35	0.036	0.17, 0.34, 0.35	0.0044
Li^+(1*H*-tetrazole)	0.36	0.14	0.18, 0.36, 0.36	0.040
Na^+(1*H*-tetrazole)	0.36	0.069	0.18, 0.36, 0.36	0.0093
K^+(1*H*-tetrazole)	0.36	0.043	0.18, 0.36, 0.36	0.0061
Li^+(2*H*-tetrazole)	0.36	0.13	0.18, 0.36, 0.37	0.044
Na^+(2*H*-tetrazole)	0.36	0.063	0.18, 0.36, 0.37	0.010
K^+(2*H*-tetrazole)	0.37	0.041	0.18, 0.36, 0.37	0.0064

[a] Active external.
[b] Inactive external.
[c] Rotational constants of the transition state treated as free internal rotors.
[d] Two-dimensional rotational constant of the transition state at threshold, treated variationally and statistically.

an average 2-D external rotational energy, as described elsewhere [3].

The model represented by Eq. (1) is expected to be appropriate for translationally driven reactions [45] and has been found to reproduce reaction cross sections well in a number of previous studies of both atom-diatom and polyatomic reactions [46,47], including CID processes [1,2,30,33–35,48–50]. It is assumed that n and σ_0 in Eq. (1) are the same for all states. The model is convoluted with the kinetic energy distribution of the reactants, and a nonlinear least-squares analysis of the data is performed to give optimized values for the parameters σ_0, E_0, and n. The error associated with the measurement of E_0 is estimated from the range of threshold values determined for different data sets, variations associated with uncertainties in the vibrational frequencies, and the error in the absolute energy scale, 0.05 eV (lab). For analyses that include the RRKM lifetime effect, the uncertainties in the reported E_0 values also include the effects of increasing and decreasing the time assumed available for dissociation (10^{-4} s) by a factor of 2.

Eq. (1) explicitly includes the internal energy of the ion, E_i. All energy available is treated statistically, which should be a reasonable assumption because the internal (rotational and vibrational) energy of the reactants is redistributed throughout the ion upon impact with the collision gas. The threshold for dissociation is by definition the minimum energy required leading to dissociation and thus corresponds to formation of products with no internal excitation. The assumption that products formed at threshold have an internal temperature of 0 K has been tested for several systems [1,2,30,33–35]. It has been shown that treating all energy of the ion (vibrational, rotational and translational) as capable of coupling into the dissociation coordinate leads to reasonable ther-

mochemistry. The threshold energies for dissociation reactions determined by analysis with Eq. (1) are converted to 0 K bond energies by assuming that E_0 represents the energy difference between reactants and products at 0 K [51]. This requires that there are no activation barriers in excess of the endothermicity of dissociation. This is generally true for ion-molecule reactions [46] and should be valid for the simple heterolytic bond fission reactions examined here [52].

3. Results

3.1. Cross sections for collision-induced dissociation

Experimental cross sections were obtained for the interaction of Xe with 12 M^+(azole) complexes, where $M^+ = Li^+$, Na^+ and K^+ and azole = imidazole, 1,2,3-triazole, 1,2,4-triazole, and tetrazole. Fig. 2 shows representative data for the 1,2,4-triazole complexes with all three metals. As discussed above, the nonzero cross sections observed in these data at the lowest energies are a consequence of multiple collisions and disappear when the data is extrapolated to zero pressure of the Xe reactant. The other azole complexes show similar relative behavior. The most favorable process for all complexes is the loss of the intact ligand in the collision-induced dissociation (CID) reactions 2.

$$M^+(\text{azole}) + Xe \rightarrow M^+ + \text{azole} + Xe \quad (2)$$

The magnitudes of the cross sections generally increase in size from M = Li to Na to K. This is largely because the thresholds decrease in this same order.

The only other products that are observed in these reactions are the result of ligand exchange processes to form M^+Xe. The cross sections for these products are one to two orders of magnitude smaller than those for the primary M^+ product and the thresholds are slightly lower (by the M^+–Xe binding energy). As little systematic information can be gleaned from these products, they were not collected in all systems and will not be discussed further.

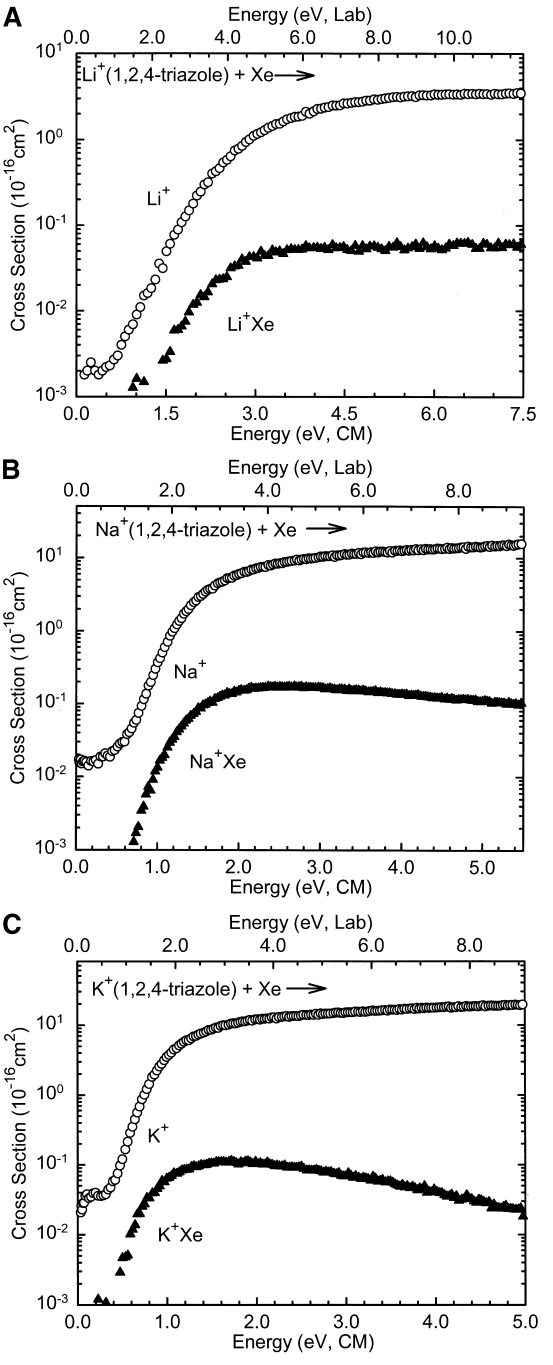

Fig. 2. Cross sections for collision-induced dissociation of M^+(1,2,4-triazole) complexes where M = Li, Na, and K [(a)–(c)] with Xe (open circles) as a function of kinetic energy in the center-of-mass frame (lower *x* axis) and the laboratory frame (upper *x* axis). Cross sections for the ligand exchange process to form M^+Xe are shown by closed triangles.

Table 3
Threshold dissociation energies at 0 K and entropies of activation at 1000 K of M^+(azole)[a]

Reactant complex	σ_0[b]	n[b]	E_0[c] (eV)	E_0 (PSL) (eV)	$\Delta S^\dagger$(PSL) (J mol^{-1} K^{-1})
Li^+(imidazole)	2.93 (0.42)	1.82 (0.08)	2.24 (0.10)	2.18 (0.10)	43 (5)
Na^+(imidazole)	13.4 (0.4)	1.36 (0.01)	1.46 (0.05)	1.45 (0.05)	36 (5)
K^+(imidazole)	41.2 (3.5)	1.17 (0.08)	1.14 (0.06)	1.13 (0.06)	27 (5)
Li^+(1*H*-1,2,4-triazole)	1.96 (0.13)	1.65 (0.05)	2.04 (0.08)	1.98 (0.08)	41 (5)
Na^+(1*H*-1,2,4-triazole)	13.6 (1.6)	1.15 (0.04)	1.30 (0.05)	1.28 (0.05)	34 (5)
K^+(1*H*-1,2,4-triazole)	18.3 (1.0)	1.14 (0.01)	0.92 (0.04)	0.90 (0.05)	26 (5)
Li^+(2*H*-1,2,3-triazole)	2.71 (0.14)	1.66 (0.04)	1.45 (0.07)	1.41 (0.08)	39 (5)
Na^+(2*H*-1,2,3-triazole)	19.0 (0.7)	1.22 (0.01)	1.00 (0.04)	0.99 (0.05)	31 (5)
K^+(2*H*-1,2,3-triazole)	14.80 (2.4)	1.44 (0.12)	0.58 (0.05)	0.57 (0.06)	24 (5)
Li^+(2*H*-tetrazole)	1.34 (0.20)	1.52 (0.06)	1.61 (0.06)	1.57 (0.07)	39 (5)
Na^+(2*H*-tetrazole)	35.3 (1.1)	1.22 (0.01)	1.21 (0.04)	1.19 (0.04)	28 (5)
K^+(2*H*-tetrazole)	37.3 (2.5)	1.18 (0.03)	0.94 (0.04)	0.92 (0.05)	23 (5)

[a] Uncertainties are listed in parentheses.
[b] Average values for loose PSL transition state.
[c] No RRKM analysis.

3.2. Threshold analysis

The model of Eq. (1) was used to analyze the thresholds for reactions 2 in 12 M^+(azole) systems. The results of these analyses are provided in Table 3 and shown in Fig. 3 for representative systems. For the triazole and tetrazole systems, we analyzed the data using molecular parameters calculated for both possible tautomers of the cationized azole dissociating to both possible tautomers of the neutral azole, four sets of parameters in all. As the vibrational frequencies are not particularly sensitive to the exact structures, the modeling parameters of Eq. (1) do not change appreciably for these various choices. In all cases, the experimental cross sections for reactions 2 in all 12 systems are accurately reproduced using a loose phase space limit (PSL) TS model [3]. Previous work has shown that this model provides the most accurate assessment of the kinetic shifts for CID processes for electrostatic ion-molecule complexes [1–3]. Good reproduction of the data is obtained over energy ranges exceeding 2 eV and cross section magnitudes of at least a factor of 100. Table 3 also includes values of E_0 obtained without including the RRKM lifetime analysis. Comparison of these values with the E_0(PSL) values shows that the kinetic shifts are small in all cases. For Li^+ complexes, the kinetic shift is 0.03–0.06 eV, while it is only 0.01–0.02 eV for the Na^+ and K^+ complexes. Although the total number of vibrations changes for the azoles (21 for imidazole, 18 for the triazoles, and 15 for tetrazole), the number of heavy atoms in these molecules (and hence, the number of lower frequency vibrations) remains the same. This explains the similarity in the kinetic shifts as the azole is varied. The rigidity of the aromatic azoles is a contributing factor to the small magnitudes of the kinetic shifts.

The entropy of activation, $\Delta S^\dagger$, is a measure of the looseness of the TS and also a reflection of the complexity of the system. It is largely determined by the molecular parameters used to model the energized molecule and the transition state, but also depends upon the threshold energy. Listed in Table 3, $\Delta S^\dagger$(PSL) values at 1000 K can be seen to decrease from the Li to the Na to the K systems. These entropies of activation can be favorably compared to $\Delta S^\dagger_{1000}$ values in the range of 29–46 J mol^{-1} K^{-1} collected by Lifshitz for several simple bond cleavage dissociations of ions [53].

3.3. Theoretical results

Theoretical structures for the neutral azoles (imidazole, 1*H*-1,2,4-triazole, 4*H*-1,2,4 triazole, 1*H*-1,2,3-triazole, 2*H*-1,2,3-triazole, 1*H*-tetrazole, and 2*H*-tetrazole) and for the complexes of all these

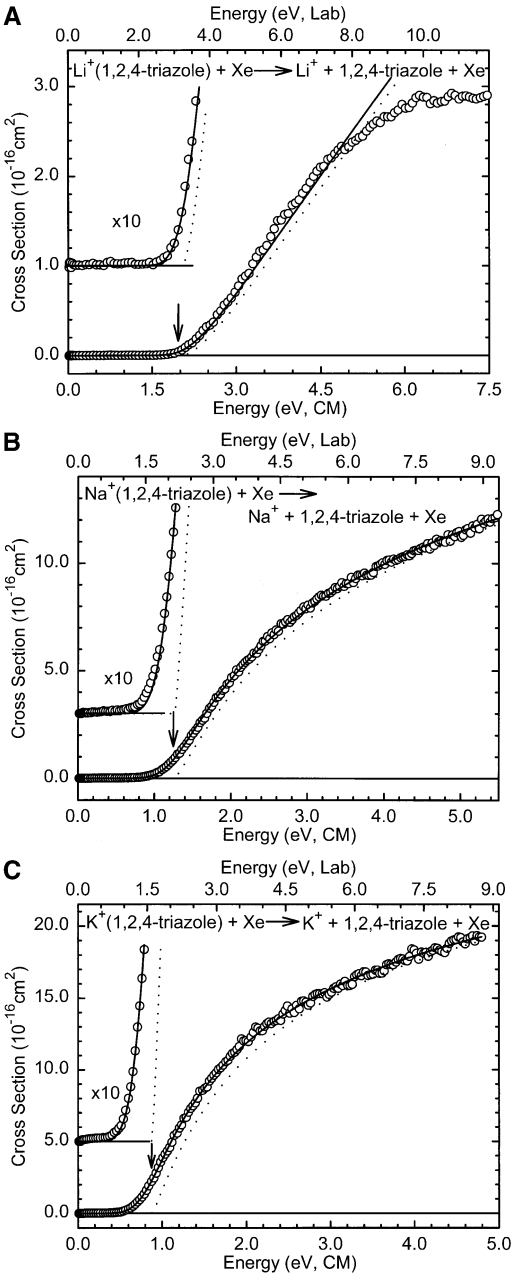

Fig. 3. Zero pressure extrapolated cross sections for collision-induced dissociation of M^+(1,2,4-triazole) complexes where M = Li, Na, and K [(a)–(c)] with Xe in the threshold region as a function of kinetic energy in the center-of-mass frame (lower *x* axis) and the laboratory frame (upper *x* axis). Solid lines show the best fits to the data using the model of Eq. (1) convoluted over the neutral and ion kinetic and internal energy distributions. Dashed lines show the model cross sections in the absence of experimental kinetic energy broadening for reactants with an internal energy of 0 K.

species with H^+, Li^+, Na^+, and K^+ were calculated at the HF 6-31G** level of theory using the Hyperchem software package [54]. Table 4 gives details of the geometries for each of these species. Results for the most stable conformations of the lithium-azole cation complexes are shown in Fig. 4. Not surprisingly, the calculations find that the proton or metal ion prefers to be bound to the nitrogen atoms for all azoles. No stable conformations corresponding to the proton or metal ion out of the plane of the azole species were found (deviations from planarity are less than 0.1° in all cases). For the imidazole, 1*H*-1,2,4-triazole, and 2*H*-1,2,3-triazole complexes, the metal binds to a single nitrogen atom, while the metal bridges two adjacent nitrogen atoms in the 4*H*-1,2,4-triazole (where the complex has C_{2V} symmetry) and 1*H*-tetrazole systems (where the binding is nearly symmetric). The 1*H*-1,2,3-triazole and 2*H*-tetrazole complexes exhibit intermediate geometries in which the metal ion lies closer to the nitrogen farthest from the amino group, which places it in better alignment with the dipole moment (see Figs. 1 and 4).

The calculated proton and metal binding energies, performed at the HF 6-31G** level including zero point energy corrections and Møller–Plesset second order perturbation (MP2) correlation energies [55–57], are listed in Tables 5 and 6, respectively. MP2 corrections could not be computed for the K^+ complexes, hence, for consistency, the discussion that follows utilizes computational results corresponding to those calculated at the 6-31G** level including zero point energy corrections, but not MP2 correlation energies, unless otherwise specified. We find that inclusion of MP2 correlation increases the calculated binding energies which leads to worse agreement with experiment because, in general calculated binding energies exceed experimentally determined binding energies even without MP2 correlation. Reasonable agreement with previous calculations performed at lower levels of theory is obtained in all cases [17,18]. The theoretical calculations accurately predict that 1*H*-1,2,4-triazole, 2*H*-1,2,3-triazole, and 2*H*-tetrazole are the most stable tautomers, by 27.2, 19.0, and 6.4 kJ/mol, respectively. For all three of these molecules, however, cations bind more strongly to the

Table 4
6-31G** geometry optimized structures of the neutral, protonated and alkali metalated azoles[a]

	Bond length (Å)									
Species	1-2	2-3	3-4	4-5	5-1	1-X	2-X	3-X	4-X	5-X
Imidazole	1.349	1.289	1.371	1.350	1.372	0.992	1.071	—	1.070	1.069
H^+(imidazole)	1.313	1.313	1.381	1.340	1.381	0.999	1.070	0.998	1.068	1.068
Li^+(imidazole)	1.328	1.306	1.384	1.344	1.373	0.996	1.071	1.930	1.069	1.068
Na^+(imidazole)	1.333	1.303	1.382	1.346	1.371	0.995	1.071	2.286	1.070	1.068
K^+(imidazole)	1.335	1.300	1.379	1.347	1.370	0.994	1.071	2.695	1.070	1.068
1*H*-1,2,3-triazole	1.318	1.266	1.356	1.356	1.343	0.993	—	—	1.068	1.068
(1,2*H*-1,2,3-triazole)$^+$	1.325	1.291	1.314	1.394	1.317	1.000	1.006	—	1.077	1.071
(1,3*H*-1,2,-triazole)$^+$	1.277	1.277	1.353	1.353	1.353	1.002	—	1.002	1.068	1.068
Li^+(1*H*-1,2,3-triazole)	1.300	1.280	1.345	1.363	1.339	0.998	2.108	1.958	1.068	1.069
Na^+(1*H*-1,2,3-triazole)	1.304	1.278	1.347	1.362	1.339	0.998	2.456	2.313	1.068	1.068
K^+(1*H*-1,2,3-triazole)	1.307	1.276	1.348	1.360	1.339	0.996	2.808	2.711	1.068	1.068
2*H*-1,2,3-triazole	1.303	1.303	1.307	1.404	1.307	—	0.992	—	1.069	1.069
Li^+(2*H*-1,2,3-triazole)	1.319	1.287	1.311	1.400	1.317	1.972	0.995	—	1.068	1.070
Na^+(2*H*-1,2,3-triazole)	1.316	1.291	1.309	1.398	1.314	2.339	0.994	—	1.068	1.070
K^+(2*H*-1,2,3-triazole)	1.314	1.294	1.308	1.400	1.313	2.792	0.994	—	1.068	1.070
1*H*-1,2,4-triazole	1.341	1.294	1.355	1.297	1.329	0.992	—	1.070	—	1.071
(1,2*H*-1,2,4-triazole)$^+$	1.344	1.318	1.315	1.315	1.318	0.999	0.999	1.071	—	1.071
(1,4*H*-1,2,4-triazole)$^+$	1.347	1.276	1.370	1.322	1.299	1.000	—	1.069	1.000	1.071
Li^+(1*H*-1,2,4-triazole)	1.340	1.283	1.370	1.316	1.311	0.997	—	1.070	1.946	1.071
Na^+(1*H*-1,2,4-triazole)	1.339	1.285	1.366	1.311	1.315	0.996	—	1.070	2.308	1.071
K^+(1*H*-1,2,4-triazole)	1.338	1.287	1.363	1.309	1.318	0.995	—	1.070	2.732	1.071
2*H*-1,2,4-triazole	1.364	1.281	1.355	1.355	1.281	—	—	1.070	0.992	1.070
Li^+(4*H*-1,2,4-triazole)	1.370	1.283	1.348	1.348	1.283	1.979	1.979	1.069	0.997	1.069
Na^+(4*H*-1,2,4-triazole)	1.371	1.284	1.349	1.349	1.284	2.332	2.331	1.069	0.996	1.069
K^+(4*H*-1,2,4-triazole)	1.369	1.284	1.349	1.349	1.284	2.718	2.718	1.069	0.996	1.069
1*H*-tetrazole	1.326	1.252	1.342	1.287	1.330	0.993	—	—	—	1.068
(1,2*H*-tetrazole)$^+$	1.323	1.266	1.289	1.321	1.314	1.003	1.004	—	—	1.070
(1,3*H*-tetrazole)$^+$	1.316	1.257	1.286	1.348	1.289	—	1.004	—	1.003	1.069
(1,4*H*-tetrazole)$^+$	1.340	1.234	1.340	1.306	1.306	1.001	—	—	1.002	1.071
Li^+(1*H*-tetrazole)	1.318	1.246	1.342	1.294	1.328	0.999	—	2.037	2.028	1.069
Na^+(1*H*-tetrazole)	1.318	1.248	1.343	1.294	1.328	0.998	—	2.366	2.400	1.069
K^+(1*H*-tetrazole)	1.319	1.250	1.343	1.294	1.328	0.997	—	2.771	2.794	1.069
2*H*-tetrazole	1.308	1.291	1.275	1.344	1.299	—	0.994	—	—	1.067
(2,3*H*-tetrazole)$^+$	1.271	1.300	1.271	1.324	1.324	—	1.005	1.005	—	1.068
Li^+(2*H*-tetrazole)	1.307	1.272	1.289	1.347	1.295	—	1.000	2.709	1.974	1.068
Na^+(2*H*-tetrazole)	1.305	1.278	1.286	1.345	1.298	—	0.999	2.852	2.325	1.068
K^+(2*H*-tetrazole)	1.303	1.282	1.283	1.344	1.299	—	0.998	2.990	2.744	1.067
	Bond angle (°)									
Species	123	234	345	451	512	X12	X23	X34	X45	X51
Imidazole	112.2	105.3	110.5	105.2	106.8	126.4	125.6	—	128.0	122.6
H^+(imidazole)	108.0	109.5	106.5	106.5	109.5	124.7	126.0	125.8	131.2	122.3
Li^+(imidazole)	111.2	105.7	109.5	105.6	108.0	125.6	125.9	124.2	128.3	122.6
Na^+(imidazole)	111.5	105.4	109.8	105.5	107.8	125.8	125.9	123.1	128.0	122.6
K^+(imidazole)	111.8	105.3	110.0	105.4	107.6	126.0	125.8	121.7	127.9	122.6
1*H*-1,2,3-triazole	108.0	109.3	108.0	103.5	111.2	119.5	—	—	130.0	123.3
(1,2*H*-1,2,3-triazole)$^+$	111.1	106.8	109.0	105.8	108.3	120.3	125.4	—	128.5	123.1
(1,3*H*-1,2,3-triazole)$^+$	104.9	113.2	104.4	104.4	113.2	118.4	—	128.4	132.4	123.3
Li^+(1*H*-1,2,3-triazole)	107.9	109.8	106.8	104.4	111.0	120.0	65.4	172.0	130.4	123.1
Na^+(1*H*-1,2,3-triazole)	107.8	109.6	107.2	104.2	111.2	119.9	68.4	169.6	130.3	123.1
K^+(1*H*-1,2,3-triazole)	107.9	109.5	107.4	104.0	111.2	119.9	72.4	169.5	130.0	123.3

(*continued*)

Table 4 (*continued*)

Species	Bond angle (°)									
	123	234	345	451	512	X12	X23	X34	X45	X51
2*H*-1,2,3-triazole	103.9	108.0	108.0	103.9	116.1	—	121.9	—	130.2	121.8
Li^+(2*H*-1,2,3-triazole)	114.9	105.5	107.6	107.9	104.1	130.3	121.5	—	130.2	122.4
Na^+(2*H*-1,2,3-triazole)	115.2	105.2	107.6	108.8	104.0	131.6	121.4	—	130.2	122.4
K^+(2*H*-1,2,3-triazole)	115.5	104.9	107.6	108.1	103.8	132.1	121.2	—	130.3	122.4
1*H*-1,2,4-triazole	102.4	115.0	102.5	110.3	109.8	120.8	—	123.0	—	123.3
(1,2*H*-1,2,4-triazole)$^+$	106.3	111.2	105.9	111.2	106.3	122.9	130.8	125.9	—	122.9
(1,4*H*-1,2,4-triazole)$^+$	104.6	110.4	106.7	106.1	112.2	119.9	—	124.1	126.2	126.9
Li^+(1*H*-1,2,4-triazole)	103.3	113.7	102.9	109.3	110.8	120.4	—	123.8	130.8	123.9
Na^+(1*H*-1,2,4-triazole)	103.1	114.1	102.7	109.6	110.6	120.5	—	123.8	131.8	123.6
K^+(1*H*-1,2,4-triazole)	103.0	114.3	102.6	109.8	110.4	120.6	—	123.7	133.4	123.5
2*H*-1,2,4-triazole	107.5	110.4	104.0	110.4	107.5	—	—	123.7	128.0	125.8
Li^+(4*H*-1,2,4-triazole)	107.8	109.3	105.9	109.3	107.8	69.7	177.5	124.5	127.0	126.2
Na^+(4*H*-1,2,4-triazole)	107.6	109.6	105.5	109.6	107.6	72.9	179.5	124.3	127.2	126.1
K^+(4*H*-1,2,4-triazole)	107.6	109.8	105.2	109.8	107.6	75.4	177.0	124.1	127.4	126.1
1*H*-tetrazole	106.7	111.4	105.8	108.2	108.0	120.9	—	—	—	125.0
(1,2*H*-tetrazole)$^+$	110.2	108.9	107.2	108.7	104.9	123.5	124.1	—	—	125.0
(1,3*H*-tetrazole)$^+$	115.8	103.5	109.9	107.8	103.0	—	121.5	—	131.3	126.8
(1,4*H*-tetrazole)$^+$	108.0	108.0	109.9	104.2	109.9	120.5	—	—	129.6	127.9
Li^+(1*H*-tetrazole)	106.0	111.7	105.8	107.0	109.4	120.4	—	70.3	176.9	125.7
Na^+(1*H*-tetrazole)	106.3	111.6	105.7	107.3	109.1	120.5	—	75.1	177.9	125.5
K^+(1*H*-tetrazole)	106.4	111.5	105.7	107.4	108.8	120.5	—	77.0	179.2	125.5
2*H*-tetrazole	114.2	106.6	106.0	112.0	101.2	—	122.4	—	—	124.1
(2,3*H*-tetrazole)$^+$	110.4	110.4	104.0	111.2	104.0	—	125.1	124.5	—	124.4
Li^+(2*H*-tetrazole)	114.7	105.6	106.5	110.7	102.1	—	122.2	43.0	143.0	124.5
Na^+(2*H*-tetrazole)	114.4	106.2	106.4	110.9	102.1	—	122.5	53.3	153.3	124.4
K^+(2*H*-tetrazole)	114.2	106.5	106.2	111.1	102.1	—	122.7	66.5	165.7	124.4

[a] The numbering scheme is shown in Fig. 1. X corresponds to atoms attached to the ring. When X is a hydrogen atom the bond length N–X is approximately 1, otherwise X = Li, Na or K.

other tautomer. This difference is easily rationalized because geometries possessing in plane lone pairs of electrons on adjacent nitrogen atoms are less stable in the neutral systems, whereas this creates a more favorable geometry for proton and metal ion binding. Thus, in the metalated systems, we find that M^+(4*H*-1,2,4-triazole) is more stable than M^+(1*H*-1,2,4-triazole) by about 31 kJ/mol, M^+(1*H*-1,2,3-triazole) is more stable than M^+(2*H*-1,2,3-triazole) by about 40 kJ/mol, and M^+(1*H*-tetrazole) is more stable than M^+(2*H*-tetrazole) by about 18 kJ/mol. These relative stability differences are not strongly dependent on the identity of the metal. Comparison of the most stable protonated complexes of each tautomer finds that (1,4*H*-1,2,4-triazole)$^+$, which can be formed from either 1*H*- or 4*H*-1,2,4-triazole, is more stable than (1,2*H*-1,2,4-triazole)$^+$ by 42.6 kJ/mole. In the 1,2,3-triazole and tetrazole systems, the most stable protonated azole can only be formed by addition of a proton to the less stable neutral tautomer. Hence, (1,3*H*-1,2,3-triazole)$^+$ is more stable than (1,2*H*-1,2,3-triazole)$^+$ by 55.2 kJ/mol, and (1,4*H*-tetrazole)$^+$ is more stable than (2,4*H*-tetrazole)$^+$ or equivalently (1,3*H*-tetrazole)$^+$ by 10.7 kJ/mol.

We can understand these trends in the binding energies by correlating the binding energies with the dipole moments of the azoles and considering the binding geometry. Fig. 5 shows that the correlation between the metal ion binding energies and dipole moments is fairly good, although there appears to be some systematic deviations from the linear trends. Bridging, found in the three more strongly bound tautomers, appears to enhance the stability, although this is partly a reflection of the larger dipole moments of these molecules. The imidazole bond energies are among the largest calculated here and show large

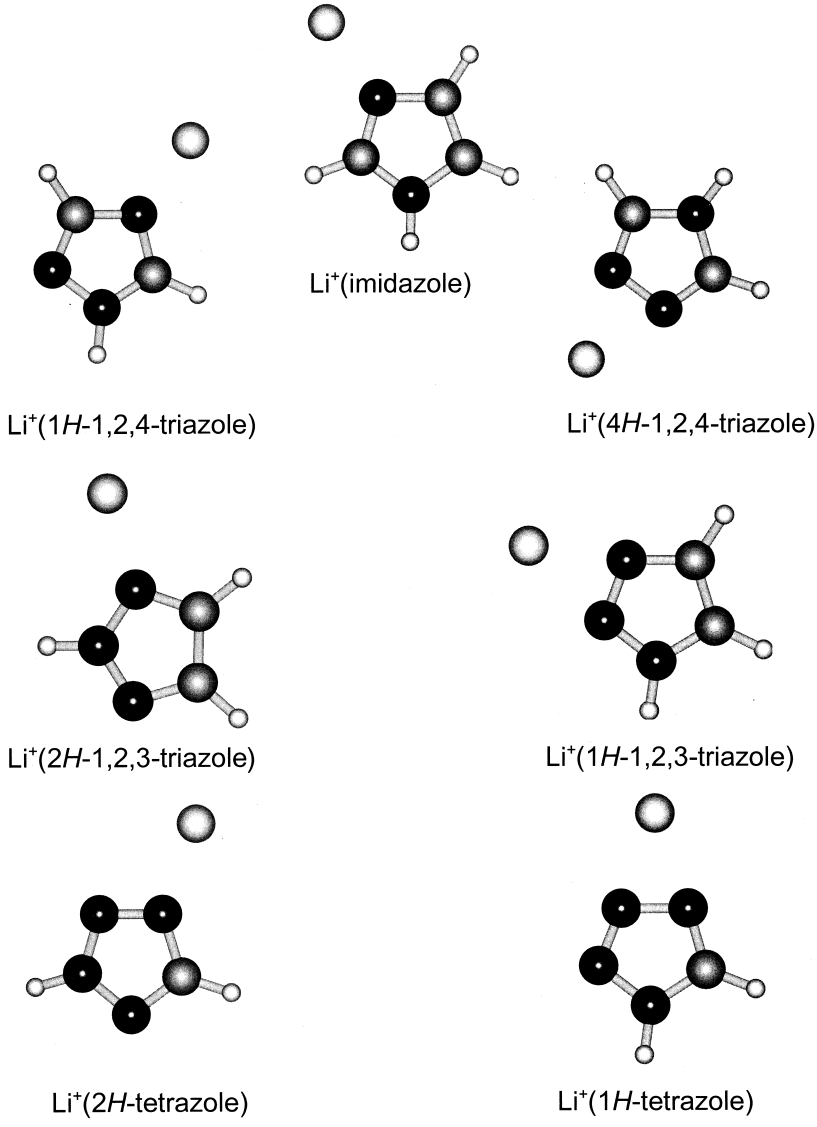

Fig. 4. Ab initio restricted Hartree Fock 6-31G**-optimized geometries of Li^+(azole) complexes where azole = imidazole, 1*H*- and 4*H*-1,2,4-triazoles, 1*H*- and 2*H*-1,2,3-triazoles, and 1*H*- and 2*H*-tetrazoles.

positive deviations from the correlation with dipole moment. We attribute this to the presence of fewer electron withdrawing groups in imidazole, compared to the other azoles, which results in a more localized electron density and stronger metal and proton binding affinity. The 4*H*-1,2,4-triazole bond energies are also particularly strong because the large dipole moment is directly aligned with the bridging binding site and neighboring CH groups are electron donors. Similarly, the 1*H*-1,2,3-triazole is slightly enhanced but the neighboring N group is an electron acceptor, weakening the metal ion affinity relative to the 4*H*-1,2,4-triazole. In contrast, binding to 1*H*-tetrazole is particularly low, a reflection of the electron withdrawing properties of the neighboring N groups in this nitrogen rich molecule. A similar correlation between dipole moment and binding energy is found in the protonated systems with somewhat larger deviations

Table 5
6-31G** calculated enthalpies of protonation of azoles in kJ/mol

Neutral azole	Site of protonation	ΔH^a	$\Delta H^{a,b}$ w/ZPEs	$\Delta H^{a,c}$ w/MP2
Imidazole	N3	1014.3	979.2	1024.4
1*H*-1,2,4-triazole	N2	906.3	875.2	904.5
1*H*-1,2,4-triazole	N4	951.3	917.8	956.5
4*H*-1,2,4-triazole	N1	980.3	944.9	987.9
1*H*-1,2,3-triazole	N2	896.5	863.2	912.5
1*H*-1,2,3-triazole	N3	954.0	918.4	967.6
2*H*-1,2,3-triazole	N1	876.1	844.2	892.7
1*H*-tetrazole	N2	821.8	788.4	826.5
1*H*-tetrazole	N3	894.5	859.0	905.0
1*H*-tetrazole	N4	903.3	869.6	902.1
2*H*-tetrazole	N1	814.1	782.0	812.9
2*H*-tetrazole	N3	807.5	775.5	830.5
2*H*-tetrazole	N4	886.8	852.6	891.4

[a] Calculated using 6-31G** frequencies scaled by 0.9.
[b] 6-31G** values including zero point energy corrections.
[c] 6-31G** values including zero point energy corrections and MP2 correlation.

from linearity. This is most likely because the proton cannot simultaneously form a strong bond to N and align itself well with the dipole moment of the molecule. In the protonated complexes, no stable conformations are found in which the proton bridges two adjacent nitrogen atoms.

Although the dipole moment explains the trends among the bond energies of the alkali ions to the various azoles, the bond energies do not disappear as the dipole moment goes to zero. This is simply because there is still an appreciable ion-induced dipole interaction between the proton or metal ion and the polarizable azoles. The variations in the polarizabilities of the azoles [58] are much smaller than the variations in the dipole moments and do not change appreciably for the various tautomers and isomers.

In all of the azole systems, the binding strength varies with the metal ion such that Li^+ binds more strongly than Na^+, which in turn binds more strongly than K^+. As these complexes are largely electrostatic in nature, this is easily understood based upon the size or equivalently the charge density on the metal. That is, the smaller the ion, the greater the charge density of the metal and therefore the greater the strength of the ion dipole interaction in these systems. The binding energy increases with decreasing charge on the metal, as shown by the correlation in Fig. 6. For a given azole, the charge retained on the metal follows the order Li < Na < K. The shorter bond distance and greater charge density in the smaller cations allows the metal ion to more effectively withdraw electron density from the neutral ligand thus reducing the charge retained on the metal and increasing the covalency of the metal-ligand interaction. The line shown in Fig. 6 is a least squares fit to all of the data. Systems lying above this line are those in which the metal ion bridges two highly basic sites, those below are those in which the metal ion binds to only one site of modest basicity.

4. Discussion

4.1. Imidazole

Imidazole is the simplest of the azole systems studied here. Tautomerization of this molecule does not lead to a unique tautomer and it possesses only a single strongly basic site (at N3). Indeed, this site is calculated to be the most basic of all the azoles considered here, having a protonation energy of 979.2 kJ/mol. The proton binds at N3 such that the protonated complex has C_{2V} symmetry. Consistent with this, we find that the metal ion binding energies for this molecule are the strongest measured here and, as expected, calculations show that the metal binds at N3. The metal is displaced slightly away from the side of the molecule containing the NH moiety, which makes it more closely aligned with the dipole moment of imidazole, 3.67 D [59]. Overall, we conclude that there is only a single possible geometry for the M^+ (imidazole) complexes. Further, because of the strong ion-dipole and ion-induced dipole interactions, the potential energy surface for M^+ + imidazole should be attractive with no barriers in excess of the bond energy. Similar considerations should hold for the other azoles in the absence of tautomerization.

The experimentally determined bond energies, equivalent to the thresholds given in Table 3, are compared with the theoretically determined bond energies at the HF 6-31G** in Table 6 and Fig. 7(a).

Table 6
6-31G** experimental and calculated enthalpies of alkali metal ion binding of M^+-azole in kJ/mol

Reaction	ΔH^a (expt.)	ΔH^b (calc.)	$\Delta H^{b,c}$ w/ZPEs	$\Delta H^{b,d}$ w/MP2
Li^+(imidazole) → Li^+ + imidazole	210.8 (9.5)	227.7	220.9	223.7
Na^+(imidazole) → Na^+ + imidazole	139.7 (5.2)	165.2	161.0	165.1
K^+(imidazole) → K^+ + imidazole	109.0 (5.6)	119.2	116.2	—
Li^+(1*H*-1,2,4-triazole) → Li^+ + 1*H*-1,2,4-triazole	191.3 (7.8)	192.3	186.5	188.3
Li^+(1*H*-1,2,4-triazole) → Li^+ + 4*H*-1,2,4-triazole	191.4 (7.8)	221.3	213.7	216.4
Li^+(4*H*-1,2,4-triazole) → Li^+ + 1*H*-1,2,4-triazole	192.2 (7.7)	222.9	218.1	222.8
Li^+(4*H*-1,2,4-triazole) → Li^+ + 4*H*-1,2,4-triazole	192.3 (7.8)	252.0	245.2	250.8
Na^+(1*H*-1,2,4-triazole) → Na^+ + 1*H*-1,2,4-triazole	123.5 (5.2)	135.1	131.5	135.1
Na^+(1*H*-1,2,4-triazole) → Na^+ + 4*H*-1,2,4-triazole	124.2 (5.0)	164.2	158.7	163.2
Na^+(4*H*-1,2,4-triazole) → Na^+ + 1*H*-1,2,4-triazole	124.4 (5.1)	166.4	164.0	164.7
Na^+(4*H*-1,2,4-triazole) → Na^+ + 4*H*-1,2,4-triazole	124.4 (5.1)	195.5	191.2	192.7
K^+(1*H*-1,2,4-triazole) → K^+ + 1*H*-1,2,4-triazole	87.0 (4.5)	93.6	91.2	—
K^+(1*H*-1,2,4-triazole) → K^+ + 4*H*-1,2,4-triazole	87.0 (4.5)	122.7	118.4	—
K^+(4*H*-1,2,4-triazole) → K^+ + 1*H*-1,2,4-triazole	86.1 (4.5)	122.6	120.9	—
K^+(4*H*-1,2,4-triazole) → K^+ + 4*H*-1,2,4-triazole	87.2 (4.5)	151.7	148.0	—
Li^+(1*H*-1,2,3-triazole) → Li^+ + 1*H*-1,2,3-triazole	136.9 (7.3)	213.3	207.5	222.1
Li^+(1*H*-1,2,3-triazole) → Li^+ + 2*H*-1,2,3-triazole	137.0 (6.9)	192.8	188.5	202.3
Li^+(2*H*-1,2,3-triazole) → Li^+ + 1*H*-1,2,3-triazole	136.4 (7.4)	172.3	166.5	173.5
Li^+(2*H*-1,2,3-triazole) → Li^+ + 2*H*-1,2,3-triazole	136.2 (7.3)	151.9	147.5	153.8
Na^+(1*H*-1,2,3-triazole) → Na^+ + 1*H*-1,2,3-triazole	95.9 (4.4)	163.5	159.8	170.8
Na^+(1*H*-1,2,3-triazole) → Na^+ + 2*H*-1,2,3-triazole	95.9 (4.4)	143.1	140.8	151.0
Na^+(2*H*-1,2,3-triazole) → Na^+ + 1*H*-1,2,3-triazole	95.7 (4.3)	122.6	118.8	126.2
Na^+(2*H*-1,2,3-triazole) → Na^+ + 2*H*-1,2,3-triazole	95.8 (4.3)	102.1	99.8	106.4
K^+(1*H*-1,2,3-triazole) → K^+ + 1*H*-1,2,3-triazole	54.7 (6.1)	124.9	121.9	—
K^+(1*H*-1,2,3-triazole) → K^+ + 2*H*-1,2,3-triazole	55.2 (5.7)	104.5	102.9	—
K^+(2*H*-1,2,3-triazole) → K^+ + 1*H*-1,2,3-triazole	54.1 (6.1)	87.2	84.3	—
K^+(2*H*-1,2,3-triazole) → K^+ + 2*H*-1,2,3-triazole	55.4 (5.5)	66.8	65.3	—
Li^+(1*H*-tetrazole) → Li^+ + 1*H*-tetrazole	153.8 (5.6)	198.1	192.6	201.0
Li^+(1*H*-tetrazole) → Li^+ + 2*H*-tetrazole	153.5 (6.0)	190.4	186.2	187.5
Li^+(2*H*-tetrazole) → Li^+ + 1*H*-tetrazole	151.4 (6.6)	182.5	175.8	189.5
Li^+(2*H*-tetrazole) → Li^+ + 2*H*-tetrazole	151.3 (6.6)	174.8	169.4	176.0
Na^+(1*H*-tetrazole) → Na^+ + 1*H*-tetrazole	114.9 (4.5)	153.9	150.3	153.0
Na^+(1*H*-tetrazole) → Na^+ + 2*H*-tetrazole	114.7 (3.7)	146.2	143.9	139.5
Na^+(2*H*-tetrazole) → Na^+ + 1*H*-tetrazole	114.6 (4.4)	134.6	130.4	137.1
Na^+(2*H*-tetrazole) → Na^+ + 2*H*-tetrazole	114.6 (3.6)	126.9	124.0	130.7
K^+(1*H*-tetrazole) → K^+ + 1*H*-tetrazole	89.2 (4.6)	118.3	115.3	—
K^+(1*H*-tetrazole) → K^+ + 2*H*-tetrazole	89.2 (4.6)	110.6	108.9	—
K^+(2*H*-tetrazole) → K^+ + 1*H*-tetrazole	89.2 (4.6)	100.5	96.7	—
K^+(2*H*-tetrazole) → K^+ + 2*H*-tetrazole	89.2 (4.6)	92.8	90.3	—

[a] Experimentally determined result when data is modelled using frequencies appropriate to the given reaction pathway.
[b] Calculated using 6-31G** frequencies scaled by 0.9.
[c] 6-31G** values including zero point energy corrections.
[d] 6-31G** values including zero point energy corrections and MP2 correlation.

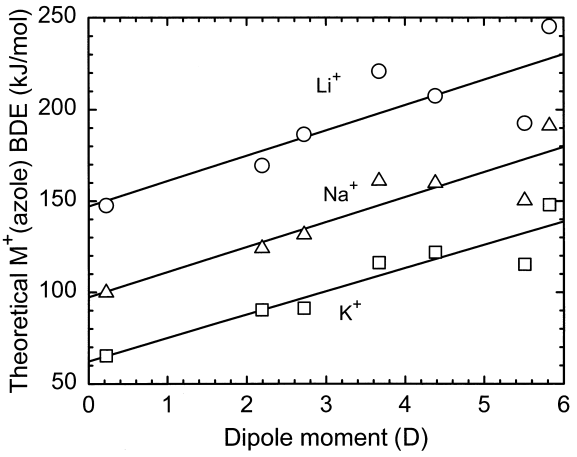

Fig. 5. Ab initio HF 6-31G** bond dissociation energies of M^+-azole (in kJ/mol) vs. dipole moment (in D, experimental values are used when available) of the neutral azole where M = Li, Na and K and azole = imidazole, 1*H*- and 4*H*-1,2,4-triazoles, 1*H*- and 2*H*-1,2,3-triazoles, and 1*H*- and 2*H*-tetrazoles. Lines are linear regression fits to the data for each metal system.

The agreement is good with the theoretical values being an average of 13 ± 7 kJ/mol (or 9 ± 6%) high. This gives us some confidence that theory can help ascertain which of the tautomers is involved in the triazole and tetrazole systems. Theoretical values from the literature [17,18] (performed at lower levels of theory) are found to have analogous trends among the metals, although in all cases, the literature values are slightly higher, such that the agreement with the present experimental values is not as good.

4.2. 1,2,4-Triazole

Proton and metal ion binding to the triazoles and tetrazole is somewhat more complicated in that all of these systems can each exist in two different tautomeric forms and possess more than one basic site. As noted in the introduction, the 1*H*-tautomer is the most stable form of the 1,2,4-triazole in both the gas phase and solid state [23–26]. Our calculations (and previous theoretical results [17]) agree with this latter conclusion, finding a stability difference of 27.2 kJ/mol. Protonation of the 1*H*-tautomer is strongly preferred at the N4 site (Table 5) and this produces the same species as protonation of the 4*H*-tautomer at N1 (or N2). In contrast, the most stable forms of the metallized 1,2,4-triazoles are distinct. In all cases, the binding energy of the 4*H*-tautomer is higher by about 30 kJ/mol for all three metals (Table 6). This can be understood by considering the dipole moments of the two tautomers, calculated to be 2.92 D (2.72 D, experimental [23,24]) for the 1*H*-tautomer and 5.82 D for the 4*H*-tautomer [58]. In addition, the metal ion is aligned with the dipole in the 4*H*-tautomer, whereas in the 1*H*-tautomer, steric interactions with the neighboring C–H bond prevent optimal orientation with the dipole moment.

On the basis of these considerations, formation of the M^+(1*H*-1,2,4-triazole) complexes should be kinetically favored in our ion source (presuming that the most stable tautomer dominates in the gas phase), while the M^+(4*H*-1,2,4-triazole) complexes are thermodynamically favored. Thus, the barrier to tautomerization in the complexes will determine the distribution of these two complexes produced in our source. Likewise, upon collisional activation, dissociation of the latter complex will have a kinetic preference to yield a 4*H*-1,2,4-triazole product, while the

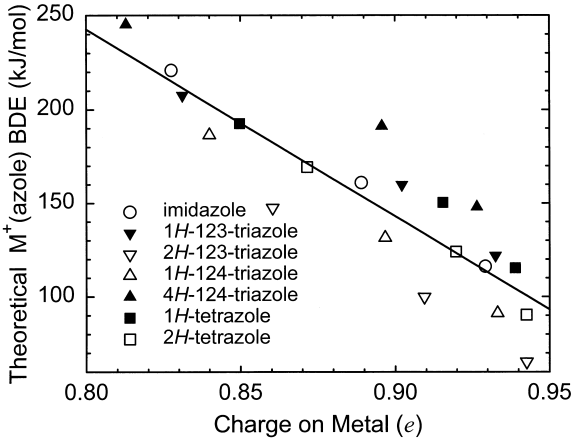

Fig. 6. Ab initio HF 6-31G** calculated bond dissociation energies of M^+-azole (in kJ/mol) vs. the charge retained on the metal in (*e*) where M = Li, Na, and K and azole = imidazole (open circles), 1*H*-1,2,4-triazole (open triangles), 4*H*-1,2,4-triazole (closed triangles), 2*H*-1,2,3-triazole (open inverted triangles), 1*H*-1,2,3-triazole (closed inverted triangles), 2*H*-tetrazole (open squares), and 1*H*-tetrazole (closed squares). The line represents a least squares fit of all of the data.

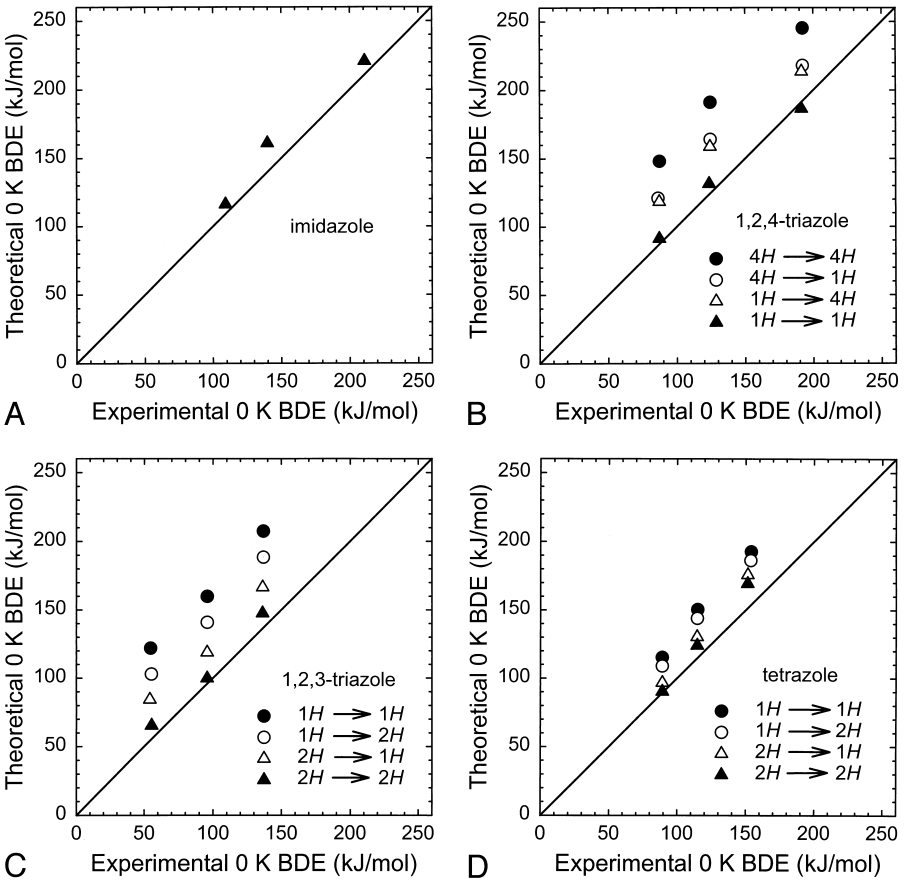

Fig. 7. Ab initio HF 6-31G** calculated bond dissociation energies (in kJ/mol) for M^+-azole where M = Li, Na, and K vs. experimentally measured bond dissociation energies (in kJ/mol) along all possible dissociation pathways. Results are shown for imidazole (a), 1,2,4-triazole (b), 1,2,3-triazole (c), and tetrazole (d). In (b)–(d), four dissociation pathways are considered. The kinetically favored dissociation pathway from each metallized tautomer is shown by closed symbols. Values corresponding to the most stable complex are shown by circles. The line indicates the values for which calculated and measured bond dissociation energies are equal. Values are taken from Table 6.

1*H*-tautomer is favored thermodynamically. Dissociation of M^+(1*H*-1,2,4-triazole) is kinetically and thermodynamically favored to form the 1*H*-1,2,4-triazole. This is shown schematically in Fig. 8.

In order to elucidate which of these various possibilities is actually occurring experimentally, we compare the CID thresholds measured (given the four possible assumptions regarding the identities of the complexes and products) with those calculated here, as shown in Fig. 7(b). In the case of the Na^+ and K^+ complexes, this comparison clearly indicates that the best agreement between experiment and theory (comparable to that found for the imidazole complexes) is obtained when the metallated and product 1,2,4-triazoles are both the 1*H*-tautomer. Here the theoretical values are an average of 6 ± 3 kJ/mol (or 6 ± 1%) high. Because this threshold is the lowest of the four possible dissociation pathways, it is possible that the M^+(4*H*-1,2,4-triazole) complexes are present and dissociate at higher collision energies. However, the modeling of these cross sections exhibits no obvious evidence for any bimodal behavior that would suggest the presence of this other tautomer. We believe that the simplest explanation for our observations is that the kinetically favored M^+(1*H*-1,2,4-triazole) complexes are the dominant species formed and that they

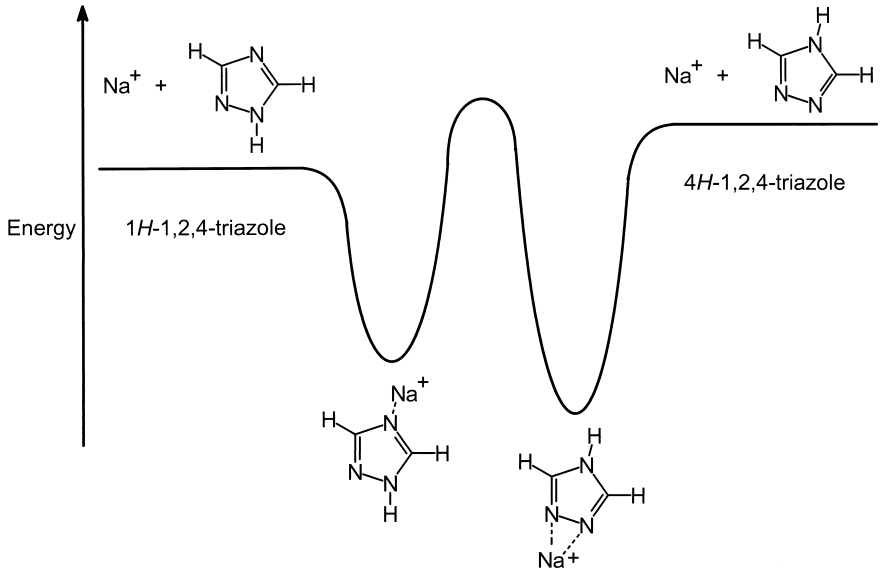

Fig. 8. Schematic potential energy surface for tautomerization of the Na^+(1,2,4-triazole) system. The barrier to tautomerization is estimated as approximately 200 kJ/mol (see text). Relative energetics of the complexes and neutral triazole tautomers are taken from calculations (Table 6).

dissociate to the ground state asymptote, M^+ + 1*H*-1,2,4-triazole. A rationalization for this behavior is given below.

In the case of the Li^+ complex, the experimentally measured bond energy is closest to the calculated dissociation enthalpy for the Li^+(1*H*-1,2,4-triazole) → Li^+ + 1*H*-1,2,4-triazole process, but slightly higher (by 4.8 kJ/mol, within the experimental error of ±7.8 kJ/mol), in contrast to the three imidazole and other 1,2,4-triazole systems which have thresholds that are slightly lower (by an average of 10 ± 7 kJ/mol) than the theoretical values. This may be an indication that a small amount of the Li^+(4*H*-1,2,4-triazole) complex is present; however, the light mass of the Li^+ product means that the octopole trapping efficiency (especially at higher kinetic energies) is not as good as for the heavier metal ions. This could also distort the shapes of the cross sections making the modeling and threshold determination slightly less accurate. Hence, we conclude that all three metal systems bind to the 1*H*-1,2,4-triazole tautomer with no tautomerization evident either upon complexation or dissociation.

4.3. 1,2,3-Triazole

As noted in the introduction, the 1*H*-tautomer is the most stable form of the 1,2,3-triazole in the solid state, while the 2*H*-tautomer is the most stable gas phase form [22]. Our calculations (and previous theoretical results [17]) agree with this latter conclusion, finding a stability difference of 19.0 kJ/mol. Protonation of either tautomer can form (1,2*H*-1,2,3-triazole)$^+$ but this species is 55.2 kJ/mol less stable than (1,3*H*-1,2,3-triazole)$^+$ which can only be formed by protonating the less stable 1*H*-tautomer. Likewise, the most stable forms of the metalated 1,2,3-triazoles are calculated to involve the 1*H*-tautomer, by about 40 kJ/mol for all three metals. This can again be understood by examining the dipole moments of the two tautomers. The symmetric 2*H*-tautomer has a small dipole, 0.22 D [22], with the negative end directed toward the NH moiety and therefore not well aligned with the binding site at N1 (or equivalently at N3). The 1*H*-tautomer has a much larger dipole, 4.38 D [22], directed between N2 and N3 (slightly displaced toward N3). Hence, binding

between the two nitrogen atoms should allow strong bonding. This is precisely what the calculations show. In the M^+(1*H*-1,2,3-triazole) complexes, the metal ions bridge N2 and N3 but the M–N2 bond lengths are slightly longer than the M–N3 bond lengths (by 0.10–0.15 Å) which provides better alignment with the dipole moment.

On the basis of these considerations, a situation similar to that observed for the 1,2,4-triazoles exists. The formation of the M^+(2*H*-1,2,3-triazole) complexes should be kinetically favored in our ion source (again presuming that the thermodynamically favored 2*H*-tautomer dominates the gas-phase species), whereas the M^+(1*H*-1,2,3-triazole) complexes are thermodynamically favored. The barrier to tautomerization will again determine the distribution of these two complexes produced under our experimental conditions. Likewise, upon collisional activation, dissociation of the latter complex will have a kinetic preference to yield a 1*H*-1,2,3-triazole product, while the 2*H*-tautomer is favored thermodynamically. Dissociation of M^+(2*H*-1,2,3-triazole) is kinetically and thermodynamically favored to form the 2*H*-1,2,3-triazole. Comparison of our experimental results with the four calculated dissociation pathways [Fig. 7(c)] again finds that the best agreement is obtained when the kinetically favored complex, M^+(2*H*-1,2,3-triazole), dissociates along the favored thermodynamic and kinetic path to M^+ + 2*H*-1,2,3-triazole. Agreement is within 11 kJ/mol for all three metals with the theoretical values being an average of 8 ± 4 kJ/mol (or 10 ± 7%) higher than the experimental results. Again it is possible that the other tautomer is present in the beam and contributes to the cross section at higher energies, but the modeling of the cross sections is straightforward and does not suggest the presence of any other species.

4.4. Tetrazole

Tetrazole is supplied as a solid of the 1*H*-tautomer, but the 2*H*-tautomer is the most stable gas phase structure [20,21]. This is confirmed by our calculations (and previous theoretical results [17,19]), although the difference in energies between the two tautomers is only 6.4 kJ/mol (13.5 kJ/mol with MP2 corrections and 7.8 kJ/mol for high level G2 calculations including zero point energy corrections [19]), much less than in the two triazole systems. Protonation of the tetrazoles is preferentially at nitrogen sites that are remote from one another, hence the most stable species are formed by protonating both tautomers at N4. The (1,4*H*-tetrazole)$^+$ formed by protonating 1*H*-tetrazole is slightly more stable, 10.6 kJ/mol, than the (2,4*H*-tetrazole)$^+$ or equivalently (1,3*H*-tetrazole)$^+$ formed by protonating 2*H*-tetrazole (Table 5). As in the two triazole systems, the most stable forms of the metallized tetrazoles are calculated to involve the less stable neutral tautomer, i.e. M^+(1*H*-tetrazole) is more stable, but only by about 18 kJ/mol for the three metal cations. Again this can be attributed to the difference in the dipole moments of the two tautomers: 2.19 D [20] (2.39 D, calculated [58]) for the 2*H*-tautomer and 5.51 D (calculated [58]) for the 1*H*-tautomer. The orientation of the dipole moments is such that binding should occur between N3 and N4 in both tautomers. Our calculations find that this is indeed the case. The bonding is quite symmetric for the M^+(1*H*-tetrazole) complexes, in that the M–N3 and M–N4 bond lengths agree within 0.04 Å for all three metal ions. In contrast, there is a strong displacement towards N4 in the M^+(2*H*-tetrazole) complexes, similar to the situation for the M^+(1*H*-1,2,3-triazole) complexes but more pronounced (see Fig. 4).

These considerations again demonstrate that formation of the M^+(2*H*-tetrazole) complexes should be kinetically favored in our ion source, while the M^+(1*H*-tetrazole) complexes are thermodynamically favored. Upon collisional activation, dissociation of the latter complex will have a kinetic preference to yield a 1*H*-tetrazole product, while the 2*H*-tautomer is favored thermodynamically. Dissociation of M^+(2*H*-tetrazole) is kinetically and thermodynamically favored to form the 2*H*-tetrazole. Because of the small energy difference in the two tautomers, the differences in the four possible dissociation pathways are much smaller for the tetrazole system than for the triazole systems (Fig. 7(d)). For comparison, the experimental bond enthalpies for the imidazole and

triazole systems (where there is little or no ambiguity in the assignment of the correct dissociation pathway) lie an average of 7 ± 6% lower than the calculated values. For the tetrazole complexes, comparison of our experimental results with the four calculated dissociation pathways again finds that the best agreement is obtained when the kinetically favored complex, M^+(2*H*-tetrazole), dissociates along the favored thermodynamic and kinetic path to M^+ + 2*H*-tetrazole. Here the theoretical values are an average of 7 ± 5% higher, in good agreement with the results for the other systems. The three other pathways are calculated to be 13 ± 4, 23 ± 2, and 28 ± 3% higher. Therefore, the threshold measurements cannot exclude the possibility that M^+(2*H*-tetrazole) could tautomerize upon dissociation to yield M^+ + 1*H*-tetrazole, but this pathway seems unlikely to be important as it is both kinetically and thermodynamically disfavored. However, the threshold comparisons allow us to confidently conclude that the observed threshold cannot correspond to dissociation of M^+(1*H*-tetrazole). Further, the modeling of the cross sections provides no evidence to support the possibility that this other tautomer is present in the beam and contributes to the cross section at higher energies.

4.5. Tautomerization barriers and complex distributions

As discussed above, the distribution of the two possible tautomeric complexes in the 1,2,3-triazole, 1,2,4-triazole and tetrazole systems produced in our experiments will be determined by the barrier to tautomerization in these complexes. A theoretical study of the tautomeric equilibrium in the neutral tetrazole systems finds that the 1,2-hydrogen shift involved has a barrier of 207 kJ/mol in the gas phase [19]. A similar barrier is expected for the analogous 1,2-hydrogen shift necessary to convert between the 1*H*- and 2*H*-tautomers of 1,2,3-triazole. Although no specific information regarding the 1,3-hydrogen shift associated with the interconversion of the 1,2,4-triazole tautomers is available to our knowledge, we anticipate that the barrier height should be comparable in magnitude based on theoretical studies of 1,2- and 1,3-sigmatropic shifts [60]. It should also be realized that the environment (solid versus liquid versus gas phase, solvent, and substituents) might significantly influence the barrier to tautomerization. Thus, in solution both tautomers are observed and the theoretical studies predict that the barrier will increase in a medium of high dielectric constant [19]. In the present work, the presence of the metal ion should influence the size of the barrier, and this effect might depend on the specific sites on the various azoles where the metal ions interact.

On the basis of these ideas, we can now understand our observations. For the complexes of all three alkali ions with the triazoles and tetrazole, we find that the thresholds measured correspond to dissociation of complexes whose formation is kinetically favored into the thermodynamically (and kinetically) favored products. This is easily rationalized by noting that a tautomerization barrier of about 200 kJ/mol greatly exceeds the binding energies measured and calculated for the sodium and potassium complexes (where the strongest bond energy is 123.5 kJ/mol) and is somewhat larger than those for the lithium complexes (strongest bond energy of 191.3 kJ/mol). This means that the potential energy surfaces involved look like those shown in Fig. 8. For the sodium and potassium systems, it is highly unlikely that the presence of the metal ion would reduce the barrier height enough to make interconversion between the two tautomeric forms feasible. Hence, the sodium and potassium complexes are exclusively species formed by association of the metal ions with the tautomer that is most stable in the gas-phase and dissociation is the reverse of this process.

The lithium ion-azole binding energies are also much smaller than the expected tautomerization barrier in the cases of 1,2,3-triazole and tetrazole. Hence, these complexes behave similarly to the sodium and potassium systems in that the measured thresholds again correspond most closely to the calculated bond energies for the species formed by association of lithium cations with the tautomer that is most stable in the gas-phase. However, in the 1,2,4-triazole system, the interaction is much stronger, such that it is feasible that the metal ion might influence the barrier height

Table 7
Enthalpies and free energies of alkali metal ion binding of M^+-azole at 298 K in kJ/mol[a]

System	ΔH^0	ΔH_0[b]	ΔH_{298}-ΔH_0[b]	ΔH_{298}	ΔH_{298}[b]	$T\Delta S_{298}$[b]	ΔG_{298}	ΔG_{298}[b]
Li^+(imidazole)	210.8 (9.5)	220.9	2.5	213.3	223.4	28.0	185.3	195.4
Na^+(imidazole)	139.7 (5.2)	161.0	1.2	140.9	162.2	27.6	113.3	134.6
K^+(imidazole)	109.0 (5.6)	116.2	0.6	109.6	116.8	26.0	83.6	90.8
Li^+(1*H*-1,2,4-triazole)	191.3 (7.8)	186.5	2.4	193.7	188.9	28.1	165.6	160.8
Na^+(1*H*-1,2,4-triazole)	123.5 (5.2)	131.5	1.1	124.6	132.6	27.6	97.0	105.0
K^+(1*H*-1,2,4-triazole)	87.0 (4.5)	91.2	0.5	87.5	91.7	26.0	61.5	65.7
Li^+(2*H*-1,2,3-triazole)	136.2 (7.3)	147.5	2.0	138.2	149.5	27.7	110.5	121.8
Na^+(2*H*-1,2,3-triazole)	95.8 (4.3)	99.8	0.8	96.6	100.6	26.9	69.7	73.7
K^+(2*H*-1,2,3-triazole)	55.4 (5.5)	65.3	0.2	55.6	65.5	25.2	30.4	40.4
Li^+(2*H*-tetrazole)	151.3 (6.6)	169.4	2.1	153.4	171.5	27.6	125.8	143.9
Na^+(2*H*-tetrazole)	114.6 (3.6)	124.0	0.8	115.4	124.8	26.2	89.2	98.6
K^+(2*H*-tetrazole)	89.2 (4.6)	90.3	0.4	89.6	90.7	25.6	64.0	65.1

[a] Uncertainties are listed in parentheses.
[b] Ab initio 6-31G** calculated values including zero point energy corrections with 6-31G** frequencies scaled by 0.9.

sufficiently that tautomerization can occur. In this regard, we note that attack at N2 should facilitate the 1,3-hydrogen shift necessary to tautomerize to 4*H*-1,2,4-triazole. However, approach of the lithium ion at N2 of 1*H*-1,2,4-triazole is disfavored at long range because it is not as well aligned with the dipole moment as attack at N4. (Theoretical calculations indicate that attachment of Li^+ at N2 is 23 kJ/mol weaker than at N4 [17]). Binding of the Li^+ at N4, which is aligned with the dipole better, should strongly inhibit the tautomerization to 4*H*-1,2,4-triazole (which now requires a 1,3 shift of both the hydrogen and lithium ion). A 1,2-hydrogen shift is feasible, but this does not produce a distinct chemical species. Overall, these considerations are consistent with the observation of a small amount of this tautomer in our experiment, induced by occasional approach of Li^+ at N2, which may help explain the slightly higher experimental threshold value obtained for this system compared to theory.

The preferential formation of higher energy species in the association of metal ions with complex organic molecules is not unique to this study. In recent work, we have observed that 12-crown-4, *c*-$(C_2H_4O)_4$, and 15-crown-5, *c*-$(C_2H_4O)_5$, form higher energy conformations when bound to Rb^+ and Cs^+, while the ground state conformations are generated when bound to Li^+, Na^+, or K^+ [61,62]. The rationalization of these observations parallels that discussed here, namely, the higher energy conformations are kinetically preferred and the barrier between the conformations can be metal ion dependent.

4.6. Conversion to 298 K and comparison to literature values

To allow comparison to previous literature values and commonly used experimental conditions, we convert the 0 K bond energies determined here to 298 K bond enthalpies and free energies. The enthalpy and entropy conversions are calculated using standard formulas and the vibrational and rotational constants given in Tables 1 and 2. Table 7 lists 0 and 298 K enthalpy, free energy, and enthalpic and entropic corrections for all systems experimentally determined (from Table 3) along with the corresponding theoretical values (from Table 6).

The free energies in Table 7 can now be compared with values taken from Alcami et al. [16] who used ion cyclotron resonance mass spectrometry to measure lithium ion transfer equilibria between reference species and imidazole, 1,2,4-triazole, and tetrazole. The experimental conditions of these experiments (e.g. temperature) are not specified although the lithium ion

affinities of the reference compounds were taken from previous experiments [63] where the temperature was 373 K. We have previously found that the absolute values from these studies are flawed [2], so that we only consider relative values among the three azoles here.

In agreement with Alcami et al., we find that imidazole is most strongly bound species, however, we find a different relative ordering for the binding of tetrazole and 1,2,4-triazole. Alcami et al. find that Li^+(imidazole) is more strongly bound than Li^+(1,2,4-triazole) by 24.3 kJ/mol, which is comparable to our $\Delta\Delta G_{298}$ value of 19.7 ± 12.3 kJ/mol derived from the information in Table 7. (Relative values at 373 K will change by less than 0.5 kJ/mol.) In turn, Alcami et al. find that Li^+(1,2,4-triazole) is **less** strongly bound than Li^+(tetrazole) by 2.5 kJ/mol, while we find it more strongly bound by 39.8 ± 10.2 kJ/mol. It is possible that Alcami et al. generate the Li^+(1*H*-tetrazole) under their experimental conditions. Indeed, theory calculates that Li^+(1*H*-1,2,4-triazole) has a binding energy 6.1 kJ/mol less than Li^+(1*H*-tetrazole). However, it is then difficult to understand why the thermodynamically favored tautomer would be formed in the tetrazole system under their experimental conditions, while the thermodynamically favored Li^+(4*H*-1,2,4-triazole) complex would not be formed. This is clearly not the case as the calculated binding energy for Li^+(4*H*-1,2,4-triazole) exceeds that of Li^+(imidazole). In conclusion, the relative values for the lithium ion affinities of imidazole and 1,2,4-triazole are in reasonable agreement with the work performed here, but the value of tetrazole is not easily reconciled.

5. Conclusions

The kinetic energy dependence of the collision-induced dissociation of M^+(azole), where M = Li, Na, and K and azole = imidazole, 1,2,3-triazole, 1,2,4-triazole, and tetrazole, with Xe are examined in a guided ion beam mass spectrometer. The dominant dissociation process in all cases is loss of the intact azole ligand. Thresholds for these processes are determined after consideration of the effects of reactant internal energy, multiple collisions with Xe, and lifetime effects (using methodology described in detail elsewhere) [3]. We also explicitly consider the possibility that tautomers may complicate the behavior in the triazole and tetrazole systems. Insight into this question is provided by ab initio calculations of all possible complexes performed at the 6-31G** RHF level of theory. We conclude that the complexes formed in the triazole and tetrazole systems correspond to association of the alkali metal cation with the most stable gas phase neutral azole (the kinetically favored tautomer) and that these complexes dissociate to the lowest energy M^+ + azole asymptote. In all cases these complexes are calculated to be the less stable tautomer. The presence of small amounts of the thermodynamically favored tautomer cannot be definitively ruled out.

Acknowledgements

Funding for this work was provided by the National Science Foundation under Grant CHE-9530412 and partial funding by the Donors of the Petroleum Research Fund, administered by the American Chemical Society.

References

[1] M.T. Rodgers, P.B. Armentrout, J. Phys. Chem. A 101 (1997) 1238.
[2] M.T. Rodgers, P.B. Armentrout, J. Phys. Chem. A 101 (1997) 2614.
[3] M.T. Rodgers, K.M. Ervin, P.B. Armentrout, J. Chem. Phys. 106 (1997) 4499.
[4] C.J. Pederson, J. Am. Chem. Soc. 89 (1957) 7017.
[5] R.M. Izatt, D.P. Nelson, J.H. Ryting, B.L. Haymore, J.J. Christensen, J. Am. Chem. Soc. 93 (1971) 1619.
[6] J.D. Cartledge, J. Midgley, M. Petrout, D. Shanson, B.G. Gazzard, J. Antimicrobial Chemotherapy 40 (1997) 517.
[7] P.C. Hopewell, Sem. Resp. Crit. Care Med. 18 (1997) 471.
[8] J.D. Cartledge, P.W. Denning, B. Dupont, N. Clumeck, S. Dewit, J. Midgley, D.A. Hawkins, B.G. Gazzard, AIDS 12 (1998) 411.
[9] Y. Hayakawa, M. Kataoka, J. Am. Chem. Soc. 119 (1997) 11 758.
[10] Y. Guo, G.A. Sulikowski, J. Am. Chem. Soc. 120 (1998) 1392.
[11] T.R. Botcher, D.J. Beardall, C.A. Wight, L. Fan, T.J. Burkey, J. Phys. Chem. 100 (1996) 8802.
[12] C. Meredith, T.P. Russell, R.C. Mowrey, J.R. McDonald, J. Phys. Chem. 102 (1998) 471.

[13] I.A. Guzel, A.G. Baboul, G.P.A. Yap, A.L. Rheingold, H.B. Schlegel, C.H. Winter, J. Am. Chem. Soc. 119 (1997) 3387.
[14] C.E. Reck, C.H. Winter, Organometallics 16 (1997) 4493.
[15] I.A. Guzei, G.P.A. Yap, C.H. Winter, Inorg. Chem. 36 (1997) 1738.
[16] M. Alcamí, O. Mó, M. Yáñez, F. Anvia, R.W. Taft, J. Phys. Chem. 94 (1990) 4796.
[17] M. Alcamí, O. Mó, M. Yáñez, J. Phys. Chem. 93 (1989) 3929.
[18] M. Alcamí, O. Mó, M. Yáñez, J. Phys. Chem. 96 (1992) 3022.
[19] M.W. Wong, R. Leung-Toung, C. Wentrup, J. Am. Chem. Soc. 115 (1993) 2465, and references therein.
[20] W.D. Krugh, L. P. Gold, J. Mol. Spec. 49 (1974) 423.
[21] A. Razynska, A. Tempczyk, E. Maslinski, J. Szafranek, Z. Grzonka, J. Chem. Soc. Perkin Trans. 2 (1983) 379; M.H. Palmer, I. Simpson, J.R. Wheeler, Z. Naturforsch. A 36 (1981) 1246.
[22] M. Begtrup, C.J. Nielsen, L. Nygaard, S. Samdal, C.E. Sjøgren, G.O. Sørensen, Acta Chem. Scand. A 42 (1988) 500.
[23] K. Bolton, R.D. Brown, F.R. Burden, A. Mishra, Chem. Comm. (1971) 873.
[24] K. Bolton, R.D. Brown, F.R. Burden, A. Mishra, J. Mol. Struct. 27 (1975) 261.
[25] P. Goldstein, J. Ladell, G. Abowitz, Acta Cryst. B 25 (1969) 135.
[26] G.A. Jeffrey, J.R. Ruble, J.H. Yates, Acta Cryst. B 39 (1983) 388.
[27] K.M. Ervin, P.B. Armentrout, J. Chem. Phys. 83 (1985) 166.
[28] R.H. Schultz, P.B. Armentrout, Int. J. Mass Spectrom. Ion Proc. 107 (1991) 29.
[29] E. Teloy, D. Gerlich, Chem. Phys. 4 (1974) 417; D. Gerlich, Diplomarbeit, University of Freiburg, Federal Republic of Germany, 1971; D. Gerlich, Adv. Chem. Phys. 82 (1992) 1.
[30] N.F. Dalleska, K. Honma, P.B. Armentrout, J. Am. Chem. Soc. 115 (1993) 12 125.
[31] N. Aristov, P.B. Armentrout, J. Phys. Chem. 90 (1986) 5135.
[32] D.A. Hales, P.B. Armentrout, J. Cluster Sci. 1 (1990) 127.
[33] N.F. Dalleska, K. Honma, L.S. Sunderlin, P.B. Armentrout, J. Am. Chem. Soc. 116 (1994) 3519.
[34] R.H. Schultz, K.C. Crellin, P.B. Armentrout, J. Am. Chem. Soc. 113 (1992) 8590.
[35] F.A. Khan, D.C. Clemmer, R.H. Schultz, P.B. Armentrout, J. Phys. Chem. 97 (1993) 7978.
[36] R.H. Schultz, P.B. Armentrout, J. Chem. Phys. 96 (1992) 1046.
[37] E.R. Fisher, B.L. Kickel, P.B. Armentrout, J. Phys. Chem. 97 (1993) 10 204.
[38] E.R. Fisher, B.L. Kickel, P.B. Armentrout, J. Chem. Phys. 97 (1992) 4859.
[39] Calculations for potassium used a 6-311G** basis set obtained from the Extensible Computational Chemistry Environment Basis Set Database, Version 1.0, as developed and distributed by the Molecular Science Computing Facility, Environmental and Molecular Sciences Laboratory which is part of the Pacific Northwest Laboratory, P.O. Box 999, Richland, Washington 99352, USA, and funded by the U.S. Department of Energy. The Pacific Northwest Laboratory is a multi-program laboratory operated by Battelle Memorial Institute for the U.S. Department of Energy under contract no. DE-AC06-76RLO 1830. Contact David Feller, Karen Schuchardt, or Don Jones for further information.
[40] D.M. Seeger, C. Korzeniewski, W. Kowalchyk, J. Phys. Chem. 95 (1991) 6871.
[41] G. Fogarasi, P. Pulay, in Vibrational Spectra and Structure, J.R. Durig (Ed.), Elsevier, New York, 1985, Vol. 14, p. 125.
[42] T.S. Beyer, D.F. Swinehart, Commun. A C M 16 (1973) 379; S.E. Stein, B.S. Rabinovitch, J. Chem. Phys. 58 (1973) 2438; Chem. Phys. Lett. 49 (1977) 1883.
[43] J.A. Pople, H.B. Schlegel, K. Raghavachari, D.J. DeFrees, J.F. Binkley, M.J. Frisch, R.F. Whitesides, R.F. Hout, W.J. Hehre, Int. J. Quant. Chem. Symp. 15 (1981) 269; D.J. DeFrees, A.D. McLean, J. Chem. Phys. 82 (1985) 333.
[44] E.V. Waage, B.S. Rabinovitch, Chem. Rev. 70 (1970) 377.
[45] W.J. Chesnavich, M.T. Bowers, J. Phys. Chem. 83 (1979) 900.
[46] P.B. Armentrout, in Advances in Gas Phase Ion Chemistry, N.G. Adams, L.M. Babcock (Eds.), JAI, Greenwich, 1992, Vol. 1, pp. 83–119.
[47] See, for example: L.S. Sunderlin, P.B. Armentrout, Int. J. Mass Spectrom. Ion Proc. 94 (1989) 149.
[48] M.B. More, E.D. Glendening, D. Ray, D. Feller, P.B. Armentrout, J. Phys. Chem. 100 (1996) 1605.
[49] D. Ray, D. Feller, M.B. More, E.D. Glendening, P.B. Armentrout, J. Phys. Chem. 100 (1996) 16 116.
[50] F. Meyer, F.A. Khan, P.B. Armentrout, J. Am. Chem. Soc. 117 (1995) 9740.
[51] See, for example: Fig. 1 in [30].
[52] P.B. Armentrout, J. Simons, J. Am. Chem. Soc. 114 (1992) 8627.
[53] C. Lifshitz, Adv. Mass Spectrom. 11 (1989) 113.
[54] Hyperchem Computational Chemistry Software Package, Version 5.0, Hypercube Inc., Gainesville, FL, 1997.
[55] C. Møller, M.S. Plesset, Phys. Rev. 46 (1934) 618.
[56] R.J. Bartlett, Ann. Rev. Phys. Chem. 32 (1981) 359.
[57] W.J. Hehre, L. Radom, P.v.R. Schleyer, J.A. Pople, Ab Initio Molecular Orbital Theory, Wiley, New York, 1986, p. 1.
[58] N.E. Kassimi, R.J. Doerksen, A.J. Thakkar, J. Phys. Chem. 99 (1995) 12 790.
[59] D. Christen, J.H. Griffiths, J. Sheridan, Z. Naturforsch. A37 (1982) 1378.
[60] F. Bernardi, M.A. Robb, H.B. Schlegel, G. Tonachini, J. Am. Chem. Soc. 106 (1984) 1198.
[61] M.B. More, D. Ray, P.B. Armentrout, J. Phys. Chem. A 101 (1997) 7007.
[62] M.B. More, D. Ray, P.B. Armentrout, unpublished.
[63] R.W. Taft, F. Anvia, J.-F. Gal, S. Walsh, M. Capon, M.C. Holmes, K. Hosn, G. Oloumi, R. Vasanwala, S. Yazdani, Pure Appl. Chem. 62 (1990) 17.